J. Appl. Comput. Mech., 5(2) (2019) 486-497
DOI: 10.22055/jacm.2018.27302.1393

ISSN: 2383-4536
jacm.scu.ac.ir

M&MoCS
Shahid Chamran University of Ahvaz
Journal of Applied and Computational Mechanics

Research Paper

Scale-Dependent Dynamic Behavior of Nanowire-Based Sensor in Accelerating Field

Alireza Yekrangisendi[1], Mojtaba Yaghobi[1], Mehran Riazian[2], Ali Koochi[3]

[1] Mechanical Engineering Group, Ayatollah Amoli Branch, Islamic Azad University, Amol, Iran
[2] Mechanical Engineering Group, Tonekabon Branch, Islamic Azad University, Tonekabon, Iran
[3] Department of Mechanical Engineering, University of Torbat Heydarieh, Torbat Heydarieh, Iran

Received October 17 2018; Revised December 01 2018; Accepted for publication December 03 2018.
Corresponding authors: Mojtaba Yaghobi, m.yaghoobi@iauamol.ac.ir; Ali Koochi, a.koochi@torbath.ac.ir

Abstract. The accelerating fields (e. g. centrifugal acceleration and constant acceleration) can change the physical performance of nano-sensors significantly. Herein, a new size-dependent model is developed to investigate the scale-dependent dynamic behavior of nanowire-fabricated sensor operated in an accelerating field. The scale-dependent equation of motion is developed by employing a consolidation of the strain gradient elasticity (SGE) and the Gurtin–Murdoch theory (GMT). A semi-analytical solution is extracted for calculating the stability parameters. Effects of different phenomena including centrifugal force, microstructure dependency, surface layer, length-scale-parameter, dispersion forces, squeezed film damping on the dynamic stability parameters are demonstrated.

Keywords: Nanowire, Accelerating field, Strain gradient elasticity, Dynamic instability, Surface energies

1. Introduction

With the novel manufacturing methods for producing ultra-small structures, the applications of nanowires and carbon nanotubes have extended rapidly in the various branch of nanotechnology [1-5]. A typical nanowire-fabricated sensor is manufactured from a deformable nanowire parallel to a solid plate. Nano-sensors have wide applications in modern measurement devices. These systems can be employed in satellites [6], automotive sensors [7], centrifugal separators [8], fault detection of roller bearing [9], CNC high-speed spindle errors detector [10], balancing power plant rotating equipment [11] and turbo-machinery angular speed detectors [12]. In these applications, the sensor operated in an accelerating field which can significantly alter the behaviour of the sensors.

The size effect (i.e. surface energies and microstructural dependency) can significantly change the mechanical performance of nano-sensors [13-16]. Various continuum theories have been presented for modelling the scale dependency of solids. An efficient theory for modelling the impacts of the surface layer on the mechanical behaviour of solids is Gurtin-Murdoch theory (GMT) [17]. For simulating the microstructural dependency the higher-order theories such as strain gradient elasticity (SGE) [15], nonlocal theory [18], couple-stress theory [19] and modified couple stress theory [20] can be employed. Among this theories, the SGE is more general and proposes some additional high order stress component in comparison with simple size-dependent models such as couple stress and modified couple stress theory. SGE can be degenerated to simplified models by neglecting this higher additional higher-order stress factors. Fu and Zhang employed GMT to study the instability of clamped-clamped nano-actuator. The pull-in behaviour of nano-actuators by considering the surface layer is investigated in Ref. [21]. Koochi et al. investigate the influence of surface energies on the electrostatic instability of NEMS operated in the Casimir regime [22]. Wang and Wang introduced a finite element simulation for incorporating the surface layer on the vibration and bending of nano-plate [23]. Shaat and Mohamed proposed a nonlinear model in the framework of the GMT and the modified couple stress theory to simulate both microstructure dependency and surface effect [24]. In Ref. [25] the pull-in of nanowire-

Published online: April 03 2019

based NEMS has been simulated using the couple stress theory and GMT. Fang et al. [26] theoretically investigate the impacts of the surface layer on the free-vibration of piezoelectric double-shell. The effect of surface energies on the vibration behaviour of the orthotropic cylindrical nano-shell is studied in Ref. [27]

In this paper, the SGE is incorporated with the GMT to extract a new model to investigate the size dependent dynamic stability of nanowire-fabricated sensor subjected to the centrifugal and constant acceleration. The influence of dispersion force and squeezed film damping are incorporated in the simulation. The dynamic instability parameters are determined using the Rayleigh-Ritz method.

2. Theory

Figure 1a depicts a typical nanowire-fabricated sensor mounted on a rotating device while Fig. 1b illustrates the two dimensional free body diagram of the sensor. The length, radius and initial gap of nano-sensor are considered to be L, *R,* and *g*, respectively. The nanowire can be assumed as a cantilever Euler beam. The displacement vector of an Euler beam can explain as [28]:

$$\mathbf{u} = -Z\frac{\partial W(X,t)}{\partial X}\mathbf{i} + W(X,t)\mathbf{k}\,. \tag{1}$$

where W is the bending of neutral axes in the Z direction.

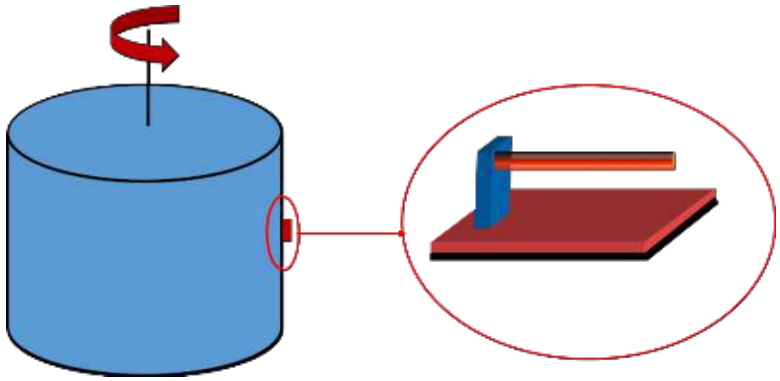

(a)

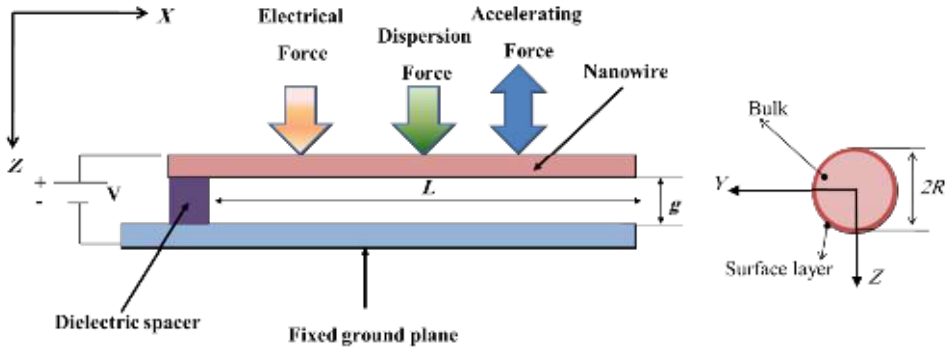

(b)

Fig. 1. a) Nano-sensor under in the centrifugal field b) A typical nanowire-fabricated sensor

2.1. Scale dependent strain energy

The scale dependent strain energy of the system (U) can be expressed as the summation of the body energy (U_B) and the surface layer energy (U_S).

$$U = U_B + U_S\,, \tag{2}$$

By incorporating the SGE and GMT the scale-dependent strain energy is obtained as:

$$U = \frac{1}{2}\int_0^L \oint_{\partial A} \tau_{ij}\varepsilon_{ij}\,dsdX + \frac{1}{2}\int_{\vartheta}\left(\sigma_{ij}\varepsilon_{ij} + p_i\gamma_i + \tau^{(1)}_{ijk}\eta^{(1)}_{ijk} + m^s_{ij}\chi^s_{ij}\right)d\vartheta\,, \tag{3}$$

The parameters of Eq. (3) can be expressed as [15, 17]:

$$\varepsilon_{ij} = \frac{1}{2}\left(u_{i,j} + u_{j,i}\right) \tag{4}$$

$$\gamma_i = \varepsilon_{mm,i} \tag{5}$$

$$\eta_{ijk}^{(1)} = \frac{1}{3}\left(\varepsilon_{jk,i} + \varepsilon_{ij,k} + \varepsilon_{ki,j}\right) - \frac{1}{15}\left[\delta_{ki}\left(\varepsilon_{mm,j} + 2\varepsilon_{mj,m}\right) + \delta_{jk}\left(\varepsilon_{mm,i} + 2\varepsilon_{mi,m}\right)\right] - \frac{1}{15}\delta_{ij}\left(\varepsilon_{mm,k} + 2\varepsilon_{mk,m}\right) \tag{6}$$

$$\chi_{ij}^{s} = \frac{1}{2}e_{jkl}u_{l,ki} \tag{7}$$

$$\sigma_{ij} = 2\mu\left(\varepsilon_{ij} + \frac{\nu}{1-2\nu}\varepsilon_{mm}\delta_{ij}\right) \tag{8}$$

$$p_i = 2\mu l_0^2 \gamma_i \tag{9}$$

$$\tau_{ijk}^{(1)} = 2\mu l_1^2 \eta_{ijk}^{(1)} \tag{10}$$

$$m_{ij}^{s} = 2\mu l_2^2 \chi_{ij}^{s} \tag{11}$$

$$\tau_{XX} = \tau_0 + E_0\left(-Z\frac{\partial^2 w}{\partial X^2}\right) \tag{12}$$

$$\tau_{nX} = \tau_0 \frac{\partial u_n}{\partial X} \tag{13}$$

where μ, ν, E_0 and τ_0 are the shear modulus, the Poisson's ratio, the surface modulus, and the surface residual stress, respectively. Furthermore, l_2, l_1, and l_0 are additional material parameters which are added to simulate the microstructure dependency. These material parameters can be evaluated experimentally [29, 30] or using molecular dynamic [31]. Zhang and Zhao employed the shifts of resonant frequencies to determine the length scale parameter [32]. The experimental observation of Al-Rub and Voyiadjis demonstrated that the length scale parameter for metals is in the between 0.2 μm to 20 μm [29]. Wang et al. measured the material length scale of Cu and Ni to be 4μm and 5μm experimentally in their work [30].

Using Eqs. (1) and (3) in combinations with Eqs. (4-13), one obtains:

$$\begin{aligned}
U &= \frac{1}{2}\int_0^L \int_A \{EZ^2(\frac{\partial^2 W}{\partial X^2})^2 + 2\mu l_0^2 Z^2(\frac{\partial^3 W}{\partial X^3})^2 + 2\mu l_0^2 Z^2(\frac{\partial^2 W}{\partial X^2})^2 + 2\mu l_2^2 Z^2(\frac{\partial^2 W}{\partial X^2})^2 + \frac{4}{25}\mu l_1^2 Z^2(\frac{\partial^3 W}{\partial X^3}) \\
&+ \frac{48}{225}\mu l_1^2(\frac{\partial^2 W}{\partial X^2})^2 + \frac{6}{25}\mu l_1^2 Z^2(\frac{\partial^3 W}{\partial X^3})^2 + \frac{1}{75}\mu l_1^2(\frac{\partial^2 W}{\partial X^2})^2 + \frac{1}{25}\mu l_1^2(\frac{\partial^2 W}{\partial X^2})^2\} dA\, dX \\
&+ \frac{1}{2}\int_0^L \oint_{\partial A}\left(-(\tau_0 + E_0\frac{\partial u_X}{\partial X})Z\frac{\partial^2 W}{\partial X^2} + \tau_0 n_Z^2(\frac{\partial W}{\partial X})^2\right) ds dX \\
&= \frac{1}{2}\int_0^L \left[\left(EI + 2\mu A l_0^2 + \frac{8}{15}\mu A l_1^2 + \mu A l_2^2\right)\left(\frac{\partial^2 W}{\partial X^2}\right)^2 + A\left(2\mu l_0^2 + \frac{4}{5}\mu l_1^2\right)\left(\frac{\partial^3 W}{\partial X^3}\right)^2\right] dX \\
&+ \frac{1}{2}\int_0^L \oint_{\partial A}\left(-(\tau_0 + E_0\frac{\partial u_X}{\partial X})Z\frac{\partial^2 W}{\partial X^2} + \tau_0 n_Z^2(\frac{\partial W}{\partial X})^2\right) ds dX
\end{aligned} \tag{14}$$

where I is the 2nd area moment and A is the cross section area.

2.2. The work of external forces

The work of external forces can evaluate by using the following equation:

$$W_{ext} = \int_0^L \int_0^W F_{ext}(X,t)\,\mathrm{d}W\ \mathrm{dX} \tag{15}$$

Here, F_{ext} is the summation of all external forces act on the sensor as follows:

$$F_{ext} = F_{elec} + F_a + \begin{cases} F_{vdW} & \text{vdw regime} \\ F_{Cas} & \text{Casimir regime} \end{cases} \tag{16}$$

where F_{elec} is the electrical force, F_{vdW} is the force due to van der Waals (vdW) attraction, F_{Cas} is the Casimir force and F_a is the force caused by accelerating field.

The external electrical potential results in a lateral force on the nanowire. This force can be evaluated by differentiating the electrical stored energy in the capacitor created by nanowire and fixed plane [25]:

$$F_{elec} = \frac{\pi\varepsilon V^2}{(g-W)\ln^2(2\frac{g-W}{R})} \tag{17}$$

where ε is the permittivity and V is the applied voltage. When the separation between the moveable wire and ground is smaller than the retardation length the vdW force, it should be considered which one is affected by the material properties. However, for long separation (i.e. the separation longer than the retardation length) the Casimir force is dominant which is not affected by the material properties [33]. For small separation, the vdW force of a wire parallel to a plate can be explained as [34]:

$$F_{vdW} = \frac{\bar{A}R^2}{(g-W)^4} \tag{18}$$

where $\bar{A}$ is the Hamaker constant. In large separations, the Casimir force is dominant and is defined as [35]:

$$F_{Cas} = \frac{\hbar c}{(g-W)^3}\frac{1}{8\pi\ln(\frac{g-W}{R})} + \frac{\hbar c}{(g-W)^3}\frac{1}{16\pi\ln^2(\frac{g-W}{R})} \tag{19}$$

where $\hbar = 1.055\times10^{-34} Js$ is the Planck constant $c = 2.998\times10^8$ m/s is the speed of light. The acceleration force per unit length (F_a) is the summation of centrifugal force and the force caused by constant accelerating field:

$$F_a = \rho A a \pm \rho A (r+g+w)\omega^2 \tag{20}$$

where r is the rotating machine radius, ω is the angular velocity of the rotary machine, and a is the constant acceleration. For the case of $g \ll r$, Eq. (20) reduces to:

$$F_a = \pi\rho R^2(a \pm r\omega^2) \tag{21}$$

It is worth to mention that the sign of centrifugal force depends on the sensor installation position. For the sensor fixed in the inner side of the machine, the centrifugal force is positive, while for the sensor mounted in the outer side of the machine the centrifugal force is negative.

2.3 The squeezed film damping and kinetic energy

The nano-sensors are frequently affected by the pressure of the gas squeezed between the nanowire and the fixed plate. The work performed by squeezed film damping can be presented as:

$$W_d = \int_0^L \int_0^W c_f \frac{\partial W(X,t)}{\partial t} dW dx \tag{22}$$

where c_f is the damping coefficients. The deflection of nano-sensor leads to an air flow over the nano-wire. The squeezed film effect between two parallel plates can be estimated through the conventional or modified Reynolds equation [36]. However, in this study, squeezed film damping coefficient is calculated by evaluating the drag force of the flow around a deflected cylinder. As the behavior of air flow changes by increasing the Stokes numbers (St), the damping coefficient is determined for low and high Stokes numbers as [37].

$$c_f = \begin{cases} 4\pi\mu_f \left(\frac{St}{2}\right)^{\frac{1}{2}} & \text{For high Stokes numbers} \\ \dfrac{4\pi\mu_f}{\log(4/St^*) - 0.0572 + 1.8K_n} & \text{For low Stokes numbers} \end{cases} \tag{23}$$

where μ_f is the viscosity, $St^* = \frac{R}{\upsilon}\frac{\partial w}{\partial t}$, υ is the momentum diffusivity and K_n is the Knudsen number. The nano-wire kinetic energy can be explained as:

$$T = \frac{1}{2}\int_0^L \int_A \rho\left[\left(\frac{\partial W(X,t)}{\partial t}\right)^2\right] dA dX \tag{24}$$

2.4. Non-dimensional energy

The total energy can evaluate by using Eqs. (14, 19, 22, 24) as:

$$\Pi = \frac{1}{2}\int_0^L\int_A \rho\left(\frac{\partial W}{\partial t}\right)^2 dA\,dX - \int_0^L (c_s + c_f)W_t W dX - \frac{1}{2}\int_0^L \oint_{\partial A}\left(-(\tau_0 + E_0 Z\frac{\partial^2 W}{\partial X^2})Z\frac{\partial^2 W}{\partial X^2} + \tau_0 n_Z^2(\frac{\partial W}{\partial X})^2\right)ds dX$$
$$-\frac{1}{2}\int_0^L\left[\left(EI + 2\mu A l_0^2 + \frac{8}{15}\mu A l_1^2 + \mu A l_2^2 + E_0 I_0\right)\left(\frac{\partial^2 W}{\partial X^2}\right)^2 + I\left(2\mu l_0^2 + \frac{4}{5}\mu l_1^2\right)\left(\frac{\partial^3 W}{\partial X^3}\right)^2\right]dX + \int_0^L\int_0^W F_{ext}(X,t)\,dW\,dX \tag{25}$$

By using Eqs. (17, 18, 19, 21) and considering $w=W/g$ and $x=X/L$ the dimensionless total energy is achieved as:

$$\bar{\Pi} = \frac{1}{2}\int_0^1\left(\frac{\partial w}{\partial \tau}\right)^2 dx - \int_0^1\int_0^w \hat{c}_f\frac{\partial w}{\partial \tau}dw\,dx - \frac{1}{2}\int_0^1 t_0\left(\frac{\partial w}{\partial x}\right)^2 dx - \frac{1}{2}\int_0^1\left[\begin{array}{l}\left(1 + e_0 + \frac{2}{15(1+\upsilon)}\left(30\left(\frac{l_0}{R}\right)^2 + 8\left(\frac{l_1}{R}\right)^2 + 15\left(\frac{l_2}{R}\right)^2\right)\right)\left(\frac{\partial^2 w}{\partial x^2}\right)^2 \\ + \frac{1}{15(1+\upsilon)(L/R)^2}\left(5\left(\frac{l_0}{R}\right)^2 + 2\left(\frac{l_1}{R}\right)^2\right)\left(\frac{\partial^3 w}{\partial x^3}\right)^2\end{array}\right]dx$$
$$+\int_0^1\int_0^w\left(\delta - \Theta\omega^2 + \frac{\eta^2}{(1-w)\ln^2(2k(1-w))} + \begin{cases}\frac{\gamma_{vdW}}{(1-w)^4} & \text{vdW } regime \\ \frac{\gamma_{Cas}\left[1 + \frac{1}{2\ln(k(1-w))}\right]}{(1-w)^3\ln(k(1-w))} & \text{Casimir } regime\end{cases}\right)dw\,dx \tag{26}$$

where:

$$k = \frac{g}{R},\quad \tau = \sqrt{\frac{E}{\rho}}\frac{R^2 t}{2L^2},\quad \eta = \frac{4\varepsilon_0 V^2 L^4}{ER^4 g^2},\quad \gamma_{Cas} = \frac{\hbar c L^4}{4\pi^2 g^4 R^4 E},\quad \gamma_{vdW} = \frac{4\bar{A}L^4}{g^5\pi R^2 E},$$
$$\hat{c}_f = \frac{2c_s L^2}{\pi R^3\sqrt{\rho E}},\quad t_0 = \frac{20\tau_0 L^2}{R^3 E},\quad e_0 = \frac{4E_0}{ER},\quad \Theta = \frac{4\rho r L^4}{ER^2 g},\quad \delta = \frac{4\rho L^4}{ER^2 g a}. \tag{27}$$

3. Solution

The Rayleigh-Ritz method (RRM) is an efficient approach for solving the nonlinear governing equation of mechanical systems. In this method, the nanowire deflection is separated to time dependent and time independent parts as:

$$w(x) = \sum_{i=1}^{N} q_i(t)\phi_i(x) \tag{28}$$

The time independent terms in the RRM should satisfy the nanowire essential boundary conditions. Therefore the mode shapes of the classical fixed-free beam are used for this purpose.

$$\phi_i(x) = \cosh(\omega_i x) - \cos(\omega_i x) - \frac{\cosh(\omega_i) - \cos(\omega_i)}{\sinh(\omega_i) - \sin(\omega_i)}\left(\sinh(\omega_i x) - \sin(\omega_i x)\right) \tag{29}$$

To find the solution, the total energy is minimized:

$$\frac{\partial \Pi}{\partial q_i} = 0 \quad i = 0,1,...,N \tag{30}$$

Equation (30) leads to the following system of ordinary differential equations:

$$\ddot{q}_i + \hat{c}\dot{q}_i + \left[1 + e_0 + \frac{2}{15(1+\upsilon)}\left(30\left(\frac{l_0}{R}\right)^2 + 8\left(\frac{l_1}{R}\right)^2 + 15\left(\frac{l_2}{R}\right)^2\right)\right]\omega_i^4 q_i$$
$$-\frac{1}{15(1+\upsilon)(L/h)^2}\left[5\left(\frac{l_0}{R}\right)^2 + 2\left(\frac{l_1}{R}\right)^2\right]\int_0^1\phi_i\frac{\partial^6}{\partial x^6}\left(\sum_{j=1}^{N} q_j\phi_j\right) - \int_0^1\phi_i\left\{t_0\sum_{j=1}^{N} q_j\frac{d^2\phi_j}{dx^2}\right\}dx$$
$$-\int_0^1\bar{F}_{ext}\phi_i\,dx + \frac{1}{15(1+\upsilon)(L/h)^2}\left(5\left(\frac{l_0}{R}\right)^2 + 2\left(\frac{l_1}{R}\right)^2\right)\frac{\partial^3}{\partial X^3}\left(\sum_{j=1}^{N} q_j\phi_j\right)\frac{d^2\phi_i}{dX^2}\Bigg|_{x=1}$$
$$-\frac{1}{15(1+\upsilon)(L/h)^2}\left(5\left(\frac{l_0}{R}\right)^2 + 2\left(\frac{l_1}{R}\right)^2\right)\frac{\partial^3}{\partial X^3}\left(\sum_{j=1}^{N} q_j\phi_j\right)\frac{d^2\phi_i}{dX^2}\Bigg|_{x=0} = 0 \qquad i = 1,2,..,N \tag{31}$$

where

$$\bar{F}_{ext} = \delta \pm \Theta\omega^2 \frac{\eta^2}{(1-\sum_{j=1}^{N} q_j \phi_j)\ln^2(2k\,(1-\sum_{j=1}^{N} q_j \phi_j))} + \begin{cases} \dfrac{\gamma_{vdW}}{(1-\sum_{j=1}^{N} q_j \phi_j)^4} & \text{vdW} \\ \dfrac{\gamma_{Cas}\left[1+\dfrac{1}{2\ln(k\,(1-\sum_{j=1}^{N} q_j \phi_j))}\right]}{(1-\sum_{j=1}^{N} q_j \phi_j)^3 \ln(k\,(1-\sum_{j=1}^{N} q_j \phi_j))} & \text{Casimir} \end{cases} \tag{32}$$

The system of differential equations is solved using the Maple software and the instability parameters are determined.

4. Results and discussion

The electromechanical instability of carbon-fabricated probe was examined experimentally by Ke et al. [38]. The gap, length, and radius of the probe are 3 μm, 6.8 μm, and 23.5 nm, respectively [38]. Figure 2 shows the distance between the free end of the moveable wire and the fixed plate for different external voltages. This figure demonstrates that the analytical size dependent nano-wire deflection is very close to the experimental data.

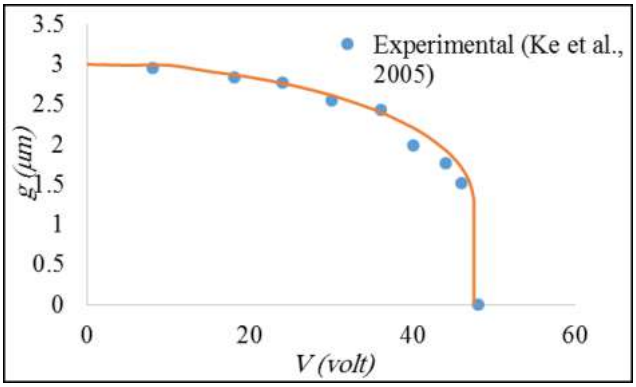

Fig. 2. The gap between the moveable electrode and the fixed plate for different voltage [38]

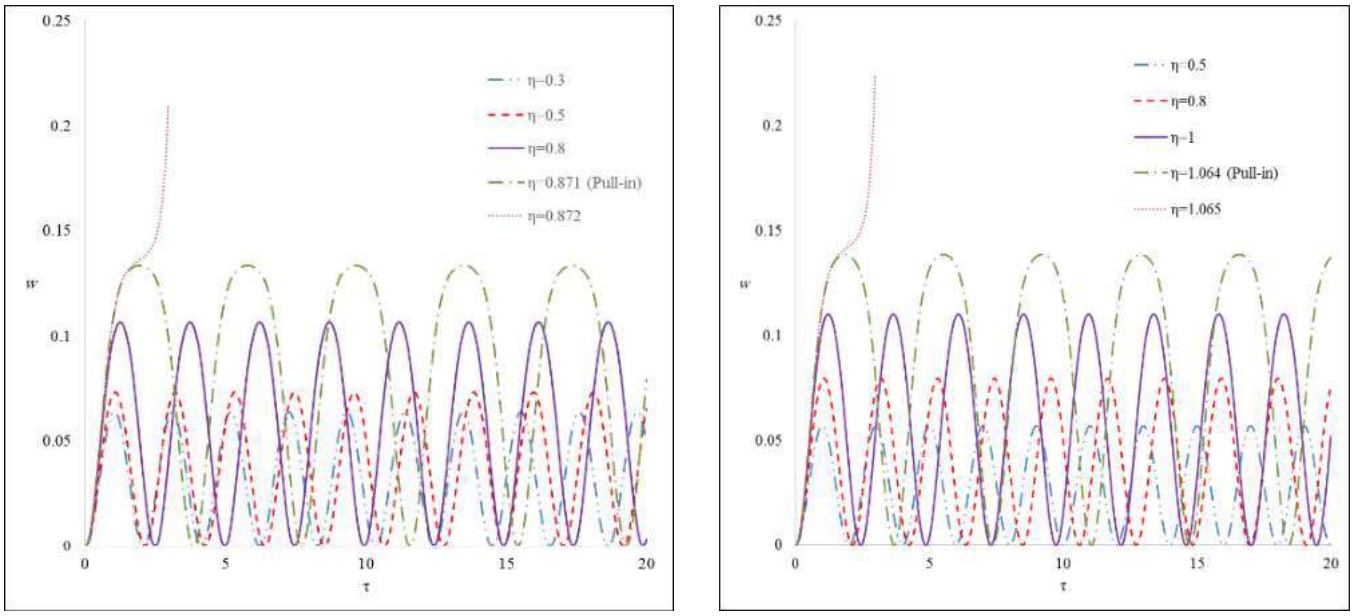

(a) (b)

Fig. 3. Time dependent deflection of nano-sensor (neglecting squeezed film damping) a) vdW regime b) Casimir regime

The dynamic behavior of nano-structures can be captured using the phase diagram [39-41]. Hence, in this paper, the dime

dependent deflections and phase diagrams of nano-switch are plotted by considering different phenomena. Figure 3 illustrates the non-dimensional deflection of nano-sensor at its free end ($w(x=1)$) as a function of dimensionless time parameter (τ). The deflection is plotted for different external voltage up to the pull-in value. This figure shows that the maximum displacement of nano-sensor raises by enhancing the voltage. When the external potential reaches the pull-in voltage, the nano-sensor tip displacement increases rapidly. The phase plane of nano-sensor damping is demonstrated in Fig. 4 neglecting the squeezed film. It is clear from this figure that the nano-sensor has an unstable saddle node and stable center point.

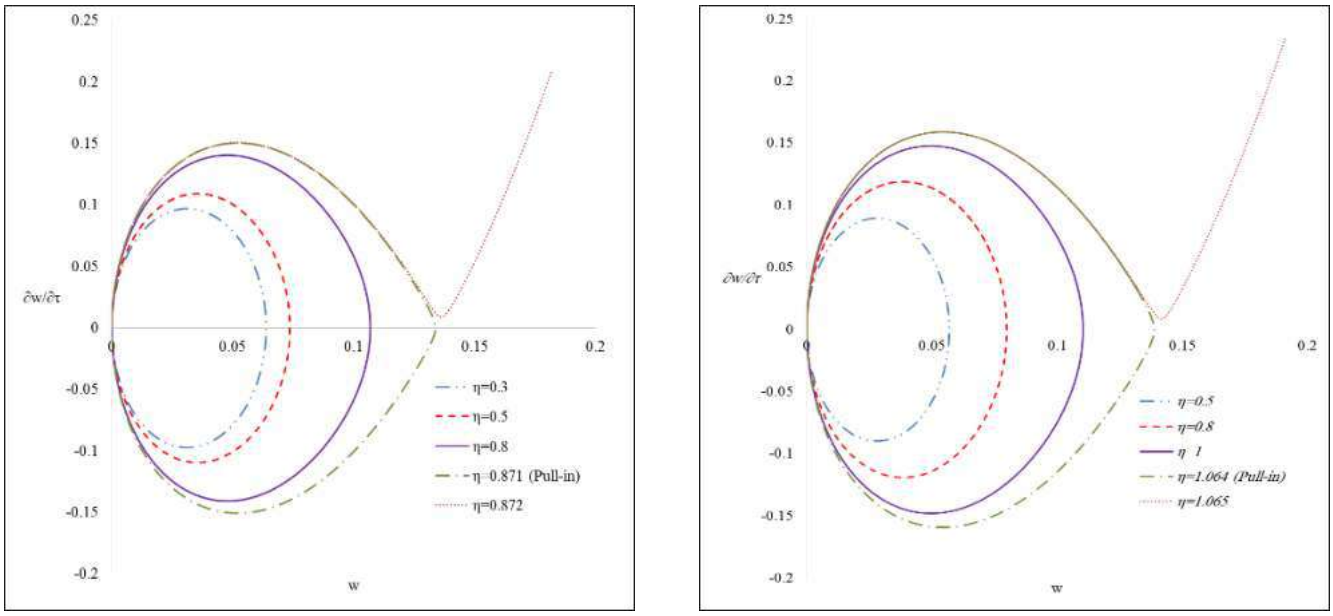

(a) (b)

Fig. 4. Phase plane of the nano-sensor by neglecting the squeezed film damping a) vdW regime b) Casimir regime

The impacts of the squeezed film damping on the non-dimensional deflection of nano-sensor at its free end ($w(x=1)$) is demonstrated in Fig. 5 as a function of dimensionless time parameter. The deflection is plotted for different external voltage up to the pull-in value. This figure reveals that similar to the undamped sensor, if the the squeezed film damping is considered, the maximum displacement of nano-sensor raises by enhancing the voltage. When the external potential reaches the pull-in value the nano-sensor tip displacement enhances rapidly. Figure 6 illustrates the effect of squeezed film damping on the phase plane of nano-sensor. It is clear from this figure that when the squeezed film damping is taken into account the stable center node converts to a stable focus one. Another fixed point is an unstable saddle node. When the applied voltage is less than the pull-in voltage the path converges to the stable focus which is due to squeezed film damping. In contrast, when the external potential is greater than the pull-in voltage the paths separate and the instability emerges.

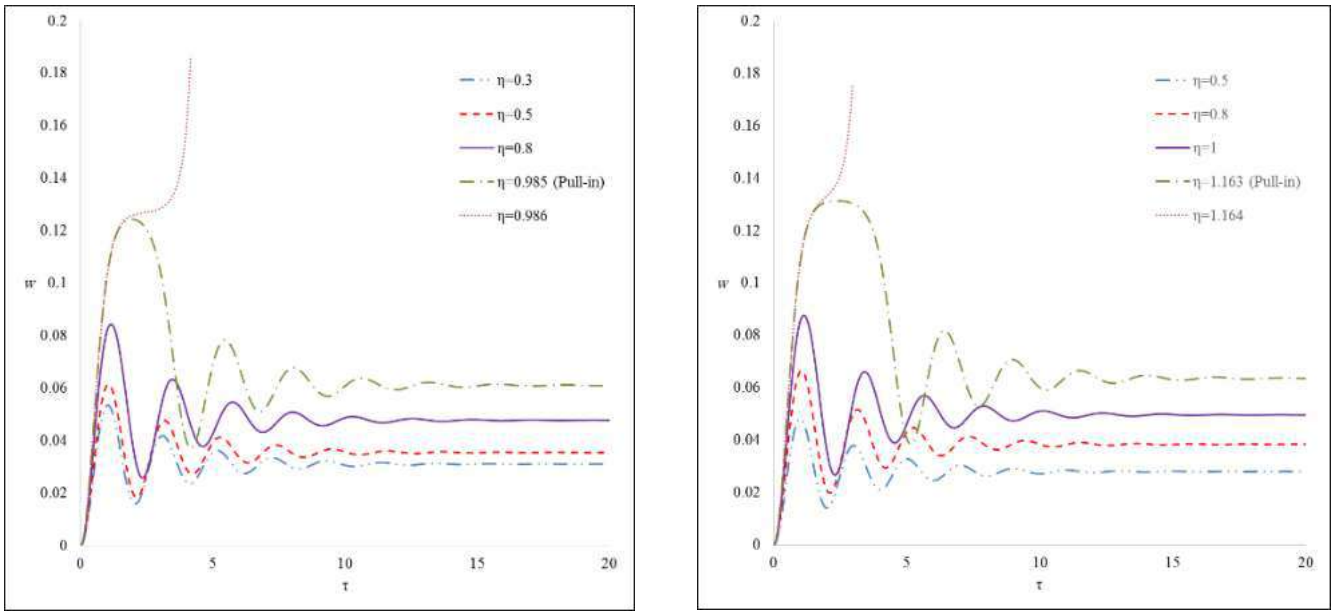

(a) (b)

Fig. 5. Effect of squeezed film damping on the time dependent deflection of nano-sensor a) vdW regime b) Casimir regime

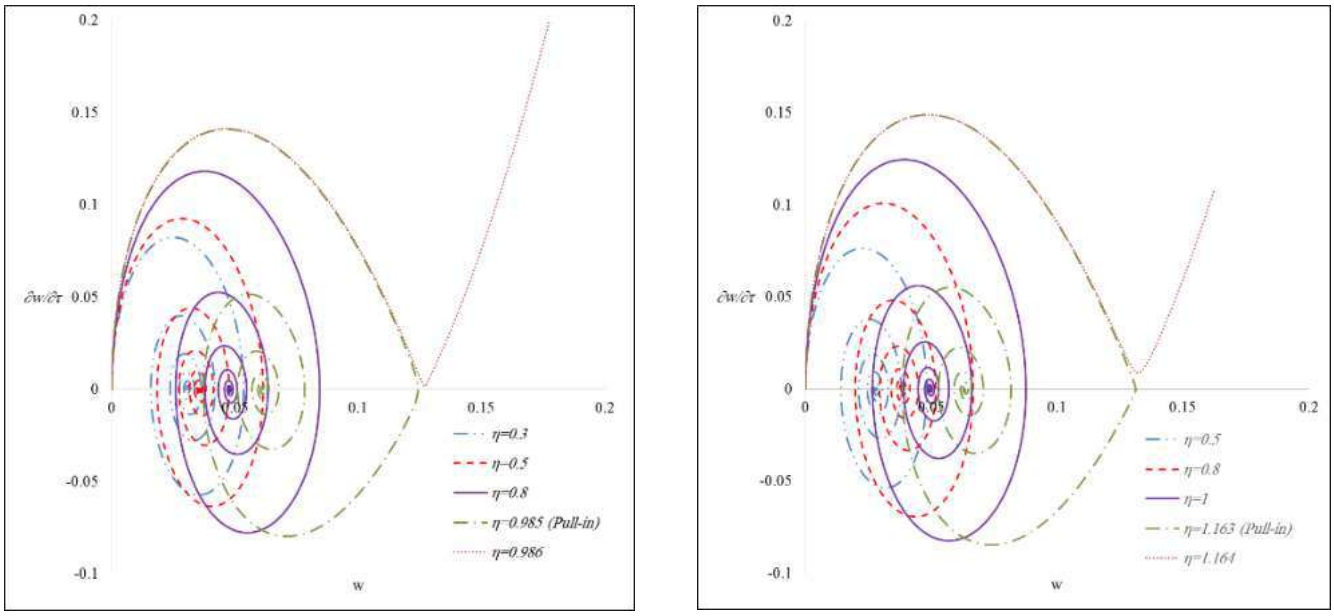

(a) (b)

Fig. 6. Impact of the squeezed film damping on the phase plane of nano-sensor a) vdW regime b) Casimir regime

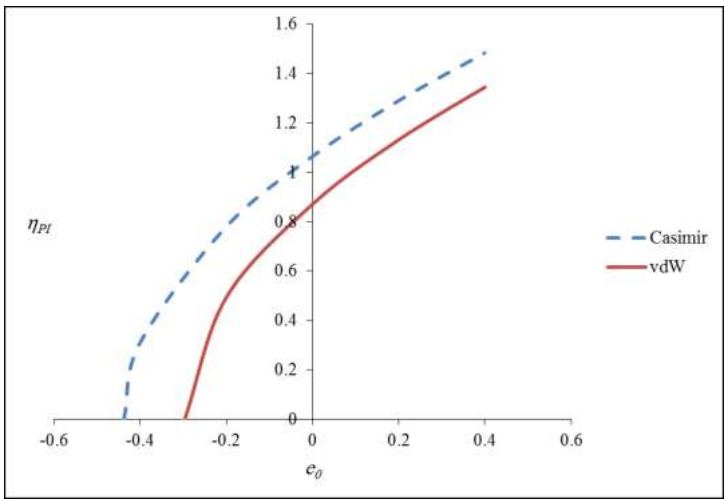

Fig. 7. Pull-in voltage of nano-sensor as a function of surface elasticity

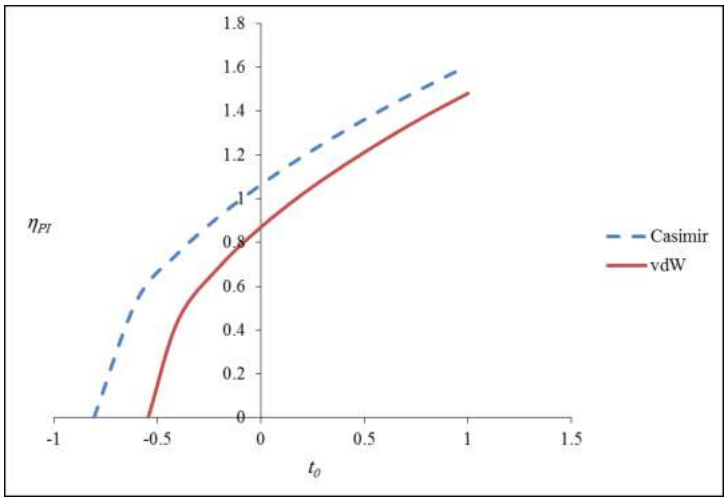

Fig. 8. Instability voltage of nano-sensor as a function of surface residual stress

To investigate the impact of surface atoms on the instability parameters, the non-dimensional instability voltage of nano-sensor is depicted as a function of surface elasticity (e_0) and surface residual stress (t_0) in Figs. 7 and 8, respectively. These

figures demonstrate the pull-in voltage of nano-sensor enhances by increasing the surface residual stress or surface elasticity. In addition, Figs. 7 and 8 show that the instability voltage of nano-sensor in the Casimir regime is greater than its instability voltage in the vdW regime.

The impact of microstructure on the instability voltage of nano-sensor is shown in Fig. 9. To this end, all length scale parameters are considered to be equal (i.e. $l_0=l_1=l_2=l$) and the non-dimensional instability voltage is determined for different l/R value. Figure 9 illustrates that the instability voltage enhances by increasing the length scale parameter.

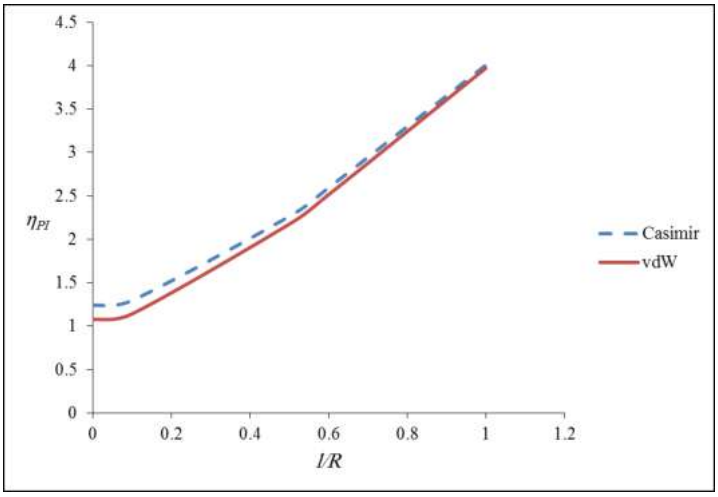

Fig. 9. Impacts of microstructure on the nano-sensor instability voltage

When the nano-sensor is attached to a rotating device, the angular velocity of the shaft can change the dynamic behavior of the sensor, significantly. Figures 10 and 11 show the time dependent deflection and phase plane of the nano-sensor for different values of angular velocities when the external voltage is equal to the pull-in value. It should be noted that the results of Fig. 10 are related to a sensor mounted inside the rotary wile Fig. 11 shows the dynamic behavior of a sensor fixed outside the rotary. In figure 10a the time history of nano-sensor at pull-in voltage is plotted while Fig. 10b demonstrates the phase diagram of nano-sensor at pull-in voltage. Figure 10a illustrates the rapid increase of the tip deflection of nano-sensor at the pull-in voltage. Moreover, it is clear from Fig. 10b that at pull-in voltage the stable center point of nano-switch becomes an unstable saddle point. This figure reveals that at pull-in point the tip velocity increases rapidly as well as tip deflection. Figure 10 shows when the nano-sensor is fixed inside the rotary, an increase in the angular velocity enhances the pull-in deflection of the nano-sensor and reduces its pull-in voltage. In contrast, when the nano-sensor is fixed outside the rotary, the pull-in time of the nano-sensor is raised by increasing the angular velocity and the pull-in phenomenon occurred at higher values of the applied potential.

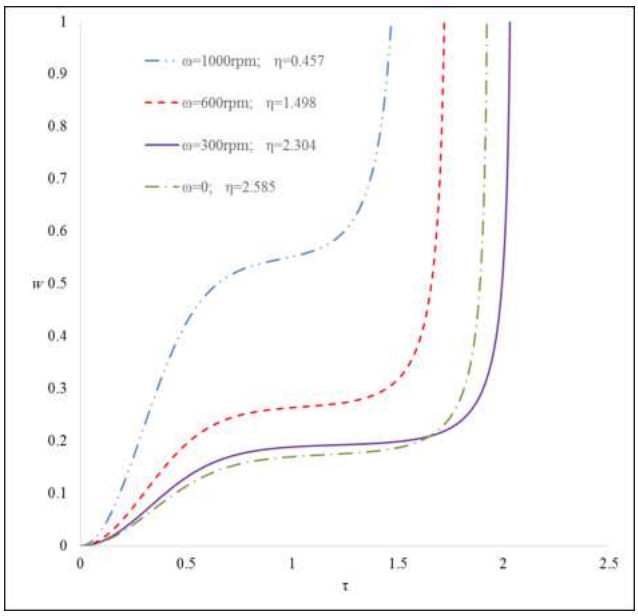

(a)

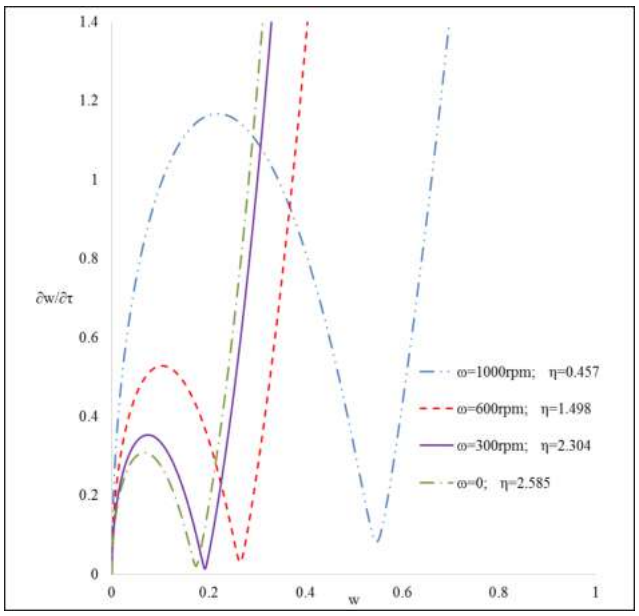

(b)

Fig. 10. Impact angular velocities on the dynamic behavior of the sensor at pull-in voltage a) Time history b) phase diagram (nano-sensor mounted inside the rotary)

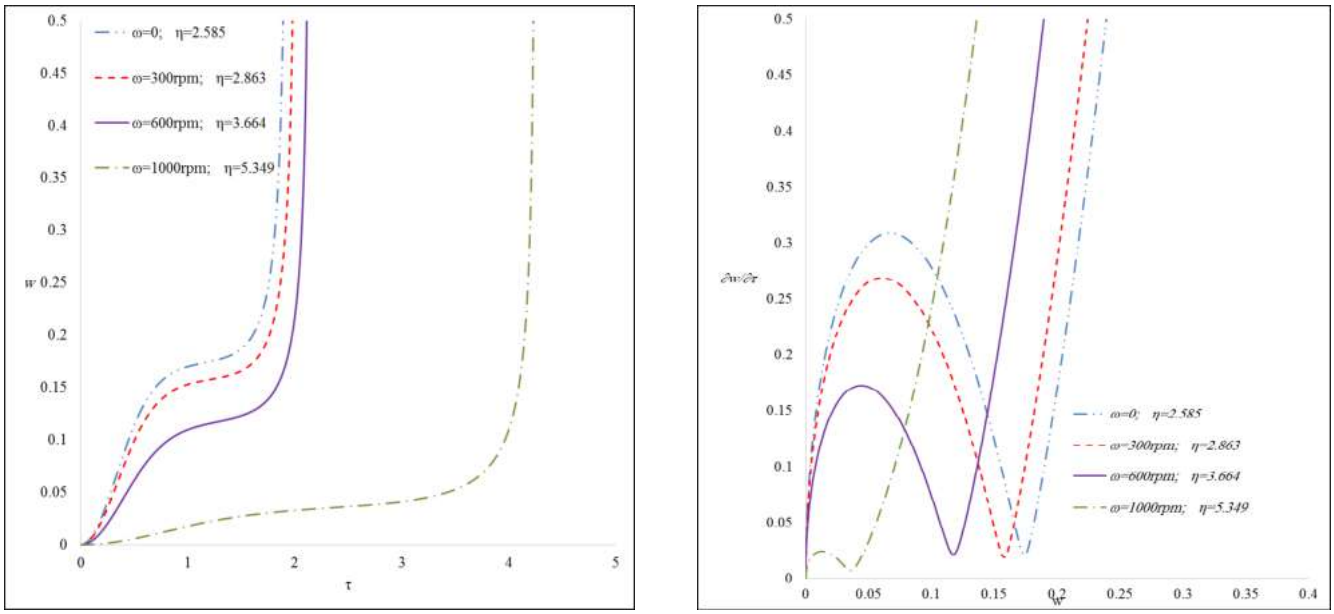

(a) (b)

Fig. 11. Impact angular velocities on the dynamic behavior of the sensor at pull-in voltage a) Time history b) phase diagram (nano-sensor mounted outside the rotary)

5. Conclusions

In this research paper, the size dependent dynamic instability of nano-wire fabricated sensor operated in an accelerating field was studied. To extract the governing equation of system, the SGE is incorporated with GMT. A semi-analytical solution method is developed using RRM and minimum energy principle. The impacts of accelerating field, squeezed film damping, the surface layer, the dispersion forces and the microstructure dependency on the dynamic instability parameters of the nano-sensor were investigated. The obtained results revealed that when the nano-sensor is fixed inside the rotary, the pull-in voltage of nano-sensor is reduced by increasing the angular velocity, however, when the nano-sensor is mounted outside the rotary the pull-in voltage of nano-sensor rises by increasing the angular velocity. Both surface energies and microstructure dependency enhance the pull-in voltage. Studing the impact of squeezed film damping reveals that by considering this phenomenon, the stable center point of the nano sensor becomes a stable focus one.

Conflict of Interest

The author(s) declared no potential conflicts of interest with respect to the research, authorship and publication of this article.

Funding

The author(s) received no financial support for the research, authorship and publication of this article.

References

[1] Akita, S., Nakayama, Y., Manipulation of nanomaterial by carbon nanotube nanotweezers in scanning probe microscope, *Japanese journal of applied physics*, 41(6S), 2002, 4242.
[2] Husain, A., Hone, J., Postma, H. W. C., Huang, X. M. H., Drake, T.; Barbic, M., Scherer, A., Roukes, M. L., Nanowire-based very-high-frequency electromechanical resonator, *Applied Physics Letters*, 83(6), 2003, 1240-1242.
[3] Li, Q., Koo, S. M., Edelstein, M. D., Suehle, J. S., Richter, C. A., Silicon nanowire electromechanical switches for logic device application, *Nanotechnology*, 18(31), 2007,315202.
[4] Feng, X. L., He, R., Yang, P., Roukes, M. L., Very high frequency silicon nanowire electromechanical resonators, *Nano Letters*, 7(7), 2007,1953-1959.
[5] Wang, G. W., Zhang, Y., Zhao, Y. P., Yang, G. T., Pull-in instability study of carbon nanotube tweezers under the influence of van der Waals forces, *Journal of Micromechanics and Microengineering*, 14, 2004,1119-1125.
[6] Fiedziuszko, S.J., Applications of MEMS in communication satellites; *13th International Conference on Microwaves, Radar and Wireless Communications*, 2000, Poland, 201-211.
[7] Fleming, W.J., Overview of automotive sensors; *IEEE Sensors Journal*, 1(4), 2001, 296-308
[8] Huang, C. T., Li, P.N., Pai, C.Y., Leu, T.S., Jen, C.P., Design and simulation of a microfluidic blood-plasma separation chip using microchannel structures, *Separation Science and Technology*, 45(1): (2009) 42–49

[9] Renaudin, L., Bonnardot, F., Musy, O., Doray, J.B., Re´mond, D., Natural roller bearing fault detection by angular measurement of true instantaneous angular speed, *Mechanical Systems and Signal Processing*, 24(7), 2010, 1998–2011.
[10] Azimloo, H., Rezazadeh, G., Shabani, R., Sheikhlou, M., Bifurcation analysis of an electro-statically actuated micro-beam in the presence of centrifugal forces, *International Journal of Non-Linear Mechanics*, 67, 2014, 7-15.
[11] Lebold, M.S., Maynard, K., Reichard, K., Trethewey, M., Bieryla, D., Lissenden, C., Dobbins, D., Using torsional vibration analysis as a synergistic method for crack detection in rotating equipment, *Aerospace conference, proceedings 2004 IEEE*, l 6, 2004, 3517–3527.
[12] Bodson, M., Chiasson, J., Novotnak, R.T., Nonlinear speed observer for high-performance induction motor control, *IEEE Transactions on Industrial Electronics,* 42(4), 1995, 337–343.
[13] Gurtin, M. E., Weissmüller, J., Larche, F., A general theory of curved deformable interfaces in solids at equilibrium, *Philosophical Magazine A*, 78(5), 1998, 1093-1109.
[14] Chen, T., Chiu, M .S., Weng, C .N., Derivation of the generalized Young-Laplace equation of curved interfaces in nanoscaled solids, *Journal of Applied Physics*, 100(7), 2006, 074308.
[15] Lam, D. C. C., Yang, F., Chong, A. C. M., Wang, J., Tong, P., Experiments and theory in strain gradient elasticity, *Journal of the Mechanics and Physics of Solids*, 51(8), 2003, 1477-1508.
[16] McFarland, A. W., Colton, J .S., Role of material microstructure in plate stiffness with relevance to microcantilever sensors, *Journal of Micromechanics and Microengineering*, 15(5), 2005, 1060.
[17] Gurtin, M.E., Murdoch, A.I., A continuum theory of elastic material surfaces, *Archive for Rational Mechanics and Analysis*, 57(4), 1975, 291-323.
[18] Eringen, A.C., Edelen, D.G.B. On nonlocal elasticity, *International Journal of Engineering Science*, 10(3), 1972, 233-248.
[19] Ejike, U.B.C.O., The plane circular crack problem in the linearized couple-stress theory, *International Journal of Engineering Science*, 7(9), 1969, 947-961.
[20] Yang, F., Chong, A.C.M., Lam, D.C.C., Tong P. Couple stress based strain gradient theory for elasticity, *International Journal of Solids and Structures*, 39(10), 2002, 2731-2743.
[21] Ma, J.B., Jiang, L., Asokanthan, S.F., Influence of surface effects on the pull-in instability of NEMS electrostatic switches, *Nanotechnology*, 21(50), 2010, 505708.
[22] Koochi, A., Kazemi, A., Khandani, F., Abadyan, M., Influence of surface effects on size-dependent instability of nano-actuators in the presence of quantum vacuum fluctuations, *Physica Scripta*, 85(3), 2012, 035804.
[23] Wang, K.F., Wang, B.L., A finite element model for the bending and vibration of nanoscale plates with surface effect, *Finite Elements in Analysis and Design*, 74, 2013, 22–29.
[24] Shaat, M., Mohamed, S. A., Nonlinear-electrostatic analysis of micro-actuated beams based on couple stress and surface elasticity theories, *International Journal of Mechanical Sciences*, 84, 2014, 208-217.
[25] Keivani, M., Mardaneh, M., Koochi, A., Rezaei, M., Abadyan, M., On the Dynamic Instability of Nanowire-Fabricated Electromechanical Actuators in the Casimir Regime: Coupled Effects of Surface Energy and Size Dependency, *Physica E*, 76, 2016, 60-69.
[26] Zhu, C. S., Fang, X. Q., Liu, J. X., Li, H. Y., Surface energy effect on nonlinear free vibration behavior of orthotropic piezoelectric cylindrical nano-shells, *European Journal of Mechanics - A/Solids*, 66, 2017, 423-432.
[27] Fang, X.Q., Zhu, C.S., Liu, J.X., Liu X.L., Surface energy effect on free vibration of nano-sized piezoelectric double-shell structures, *Physica B: Condensed Matter*, 529, 2018, 41-56
[28] Dym, C. L., Shames, I. H., *Solid Mechanics: A variational Approach*. Railway Publishing House, Beijing, China, 1984.
[29] Al-Rub, R.K.A., Voyiadjis, G.Z., Determination of the Material Intrinsic Length Scale of Gradient Plasticity Theory, *International Journal for Multiscale Computational Engineering*, 29(3), 2004, 377-400
[30] Wang, W., Huang, Y., Hsia, K.J., Hu, K.X., Chandra, A., A study of microbend test by strain gradient plasticity, *International Journal of Plasticity*, 19, 2003, 365–382
[31] Maranganti, R., Sharma, P., A novel atomistic approach to determine strain-gradient elasticity constants: tabulation and comparison for various metals, semiconductors, silica, polymers and the (Ir) relevance for nanotechnologies, *Journal of the Mechanics and Physics of Solids,* 55(9), 2007, 1823-52
[32] Zhang, Y., Zhao, Y. P., Measuring the nonlocal effects of a micro/nanobeam by the shifts of resonant frequencies, *International Journal of Solids and Structures*, 102-103, 2016, 259-266.
[33] Zhao, Y.P., Wang, L.S.; Yu T.X., Mechanics of adhesion in MEMS—a review, *Journal of Adhesion Science and Technology*, 17, 2003, 519-546.
[34] Keivani, M., Koochi, A., Abadian, N., Rezaei, M., Abadyan, M., Static and dynamic instability of nanowire-fabricated nanoelectromechanical systems: effects of flow damping, van de Waals force, surface energy and microstructure, *Canadian Journal of Physics*, 94(6), 2016, 594-603
[35] Keivani, M., Koochi, A., Abadyan, M., A new model for stability analysis of electromechanical nano-actuator based on Gurtin-Murdoch and consistent couple-stress theories, *Journal of Vibroengineering*, 18(3), 2016, 1406-1416.
[36] Feng, C., Zhao, Y.P., Liu D.Q., Squeeze-film effects in MEMS devices with perforated plates for small amplitude vibration, *Microsystem Technologies,* 13(7), 2007, 625–633.
[37] Berli, C.L., Cardona A. On the calculation of viscous damping of microbeam resonators in air, *Journal of Sound and Vibration*, 18(3), 2009, 249-253.
[38] Ke, C.H., Pugno, N., Peng, B., Espinosa, H.D., Experiments and modeling of carbon nanotube-based NEMS devices, *Journal of the Mechanics and Physics of Solids*, 53(6), 2005, 1314-1333.

[39] Lin, W.H., Zhao Y.P., Dynamics behavior of nanoscale electrostatic actuators. Chinese Physics Letters, 20(11), 2003, 2070-2073
[40] Lin, W.H., Zhao Y.P., Nonlinear behavior for nanoscales electrostatic actuators with Casimir force, *Chaos, Solitons & Fractals*, 23, 2005, 1777–1785
[41] Lin, W.H., Zhao Y.P. Casimir effect on the pull-in parameters of nanometer switches, *Microsystem Technologies*, 11, 2005, 80-85.